Critical behavior of magnetoresistance near the metal–insulator transition of $La_{0.7}Ca_{0.3}MnO_3$

H. Huhtinen[a],*, R. Laiho[a], K.G. Lisunov[b], V.N. Stamov[b], V.S. Zakhvalinskii[b]

[a] *Wihuri Physical Laboratory, Department of Physics, University of Turku, FIN-20014 Turku, Finland*
[b] *Institute of Applied Physics, Academiei Str. 5, MD-2028 Kishinev, Moldova*

Abstract

The resistivity, $\rho(T)$, of thin film and bulk samples of $La_{0.7}Ca_{0.3}MnO_3$ is investigated in magnetic fields between 0–10 T and temperatures between 10–340 K. Metallic resistivity, $\rho_{lt}(T) = \rho_r + \rho_2 T^2 + \rho_{4.5} T^{4.5}$, is observed well below the metal–insulator transition (MIT) temperature T_{MI}. For $T > T_{MI}$, the resistivity is governed by the Shklovskii-Efros variable-range hopping mechanism, giving $\rho_{ht}(T) = \rho_0 \exp[(T_0/T)^{1/2}]$. Combining the contributions of itinerant and localized carriers, that means $\rho_{lt}(T)$ and $\rho_{ht}(T)$, respectively, a good fit of $\rho(T)$ is obtained over the whole temperature region investigated. Below MIT, for $T \rightarrow T_{MI} - 0$, a critical behavior obeying the law $\rho(T) \sim (T_{MI} - T)^{-v}$ is observed. For $T \rightarrow T_{MI} + 0$, the critical behavior of the resistivity is determined by divergence of the correlation length $\xi \sim (T - T_{MI})^{-v}$, due to the relation $T_0 \sim 1/\xi$. In both cases, $v \approx 1$. The temperature dependence of ξ, when approaching T_{MI} from the high-temperature side, is attributed to generation of critical clusters of the metallic phase in the semiconductor matrix. Rapid increase of the metallic component is observed when B is increased. © 2002 Elsevier Science B.V. All rights reserved.

1. Introduction

The mixed-valence perovskite compound $La_{1-x}Ca_xMnO_3$, briefly LCMO, has attracted a lot of attention due to the large drop of the resistivity, ρ, in the external magnetic field. This effect appears around the metal–insulator transition (MIT) temperature, T_{MI}, which is close to the paramagnetic–ferromagnetic Curie temperature, T_C, and attains a maximum near $x \approx 0.33$ [1]. The close interplay between magnetic and transport properties of LCMO and the related "colossal" magnetoresistance (CMR) materials is basically explained by competing antiferromagnetic (AFM) Mn^{3+}–Mn^{3+} superexchange and ferromagnetic (FM) Mn^{3+}–Mn^{4+} double exchange interactions, accompanied by the Jahn–Teller effect [2]. As a consequence of local Jahn–Teller distortions, a polaronic state can appear and play an important role in the transport properties of LCMO (see e.g. Refs. [3–6]).

*Corresponding author. Tel.: +358-2-333-59-43; fax: +358-2-231-9836.

E-mail address: hannu.huhtinen@utu.fi (H. Huhtinen).

Attempts to interpret CMR by polaronic effects, including the magnetic polaron mechanism [7], the composite polaron mechanism [8] and bipolaron to polaron dissociation [9], focus attention on the microscopic nature and the magnetic field dependence of the MIT. On the other hand, valuable phenomenological approaches have been developed to describe the resistivity of CMR materials in a wide temperature interval above and below MIT by combining metallic-like and hopping conductivity of itinerant and localized carriers. Accordingly, two-component polaronic transport, including large itinerant polarons stable at low temperatures and small localized polarons stable at high temperatures, has been suggested [10]. An effective-medium approach has been used to compute the total resistivity of the two-component system in the mean-field approximation by assuming the coexistence of localized and itinerant carriers near T_C in an LCMO film with $x = 0.3$ [11]. The model of parallel conduction channels has also been applied to thin $La_{0.5}Sr_{0.5}MnO_{3-\delta}$ films [12] and LCMO ceramic samples [13]. The physical basis of these models is the intrinsic phase separation due to charge, orbital and spin-ordering effects in manganite perovskite CMR materials [14–16]. The phenomenological analyses, however, remove the attention away from the MIT region to the behavior of $\rho(T)$ at asymptotically high- and low-temperatures.

In this paper, we investigate the magnetoresistance of $La_{0.7}Ca_{0.3}MnO_3$ thin film and bulk ceramic samples, paying special attention to the critical behavior of $\rho(T)$ in the vicinity of MIT. Such investigations are expected to yield valuable information on microscopic processes governing the transport phenomena.

2. Results and discussion

2.1. Experimental details

Bulk LCMO samples were prepared from ceramic material synthesized by heating stoichiometric mixtures of La_2O_3, $CaCO_3$ and MnO_2 in air at first for 35 h at 1320°C and then for 22 h at 1375°C, with intermediate grindings. The films were deposited on $NdGaO_3$ (1 0 0) substrates with a XeCl laser ($\lambda = 308$ nm) at the pulse power density of 2 J/cm². The substrate temperature was 700°C and the oxygen pressure in the deposition chamber was 0.25 Torr. The films were square-shaped having the area of 11.7 mm² and thickness of 200 nm as determined from the edge of the film by atomic force microscopy.

Measurements of $\rho(T)$ were made with the four-probe technique in the transverse magnetic field configuration ($\mathbf{B} \perp \mathbf{j}$) for B between 0 and 10 T. The sample probe was inserted in a He exchange gas dewar, where its temperature could be varied between 10 and 340 K to an accuracy of 0.5%. No difference was observed between the $\rho(T)$ curves measured by increasing and decreasing T or for B, parallel and perpendicular to the film plane.

The absolute values of the resistivity and the shapes of the $\rho(T)$ curves shown in Fig. 1 resemble closely those values published earlier for LCMO thin films and bulk samples with $x \approx 0.3$ (see e.g. Refs. [1,17,18]). The value of T_{MI}, determined by inflection of the $\rho(T)$ curve measured at low B, is close to T_C and increases with increasing B. The maximum drop of the resistivity at $B = 8$ T, $[\rho(8T) - \rho(0)]/\rho(0)$ is -92% in the film at $T = 252$ K and -74% in the bulk sample at $T = 257$ K. The resistivity peak is broader, the drop of $\rho(T)$ below the peak is sharper, and the

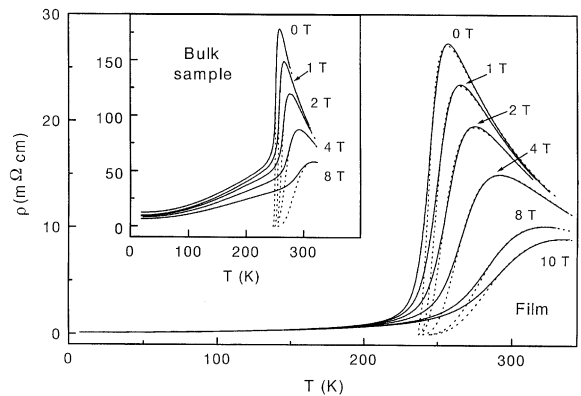Fig. 1. Temperature dependence of the resistivity, ρ, of a thin film and a bulk sample (inset) of $La_{0.7}Ca_{0.3}MnO_3$ in different magnetic fields. The dashed curves are calculated using Eqs. (1) and (6) as described in the text.

dependence on B with decrease in T is much smaller in the film than in the bulk sample.

2.2. Temperature dependence of ρ far from MIT

It is widely believed that the semiconductor-like behavior of $\rho(T)$ above T_{MI} in perovskite manganites is connected with small polaron hopping obeying a simple Arrhenius law [19–21]. On the other hand, clear deviations from this law have been observed both in bulk and thin film samples of different CMR materials [22,23]. In these papers, the Mott mechanism [24] of the variable-range hopping (VRH) conductivity has been utilized, paying less attention to the Shklovskii-Efros (SE) mechanism [25]. The latter sets in when the Coulomb interaction between the charge carriers is important, leading to a soft gap in the spectrum of the density of states around the Fermi level. The resistivity can be expressed in a universal form

$$\rho_{ht}(T) = \rho_0 \exp\left[\left(\frac{T_0}{T}\right)^p\right], \tag{1}$$

where ρ_0 depends weakly on T and T_0 is the characteristic VRH temperature. The Arrhenius law, which is related to the nearest-site hopping, corresponds to $p = 1$. The Mott and the SE–VRH conductivity, are obtained with $p = \frac{1}{4}$ and $\frac{1}{2}$, respectively. In Fig. 2 (upper panel), the plots of $\ln \rho$ vs. $T^{-1/2}$ and $T^{-1/4}$, having linear parts of the same quality without allowing selection between the Mott and the SE–VRH mechanisms are shown. In such a situation, the local activation energy [25]

$$E_{loc}(T) = \frac{d \ln \rho_{ht}(T)}{d(1/kT)} \tag{2}$$

can be used for identification of the type of hopping. When T_0 does not depend on T and the weak temperature dependence of ρ_0 is neglected, the slope of the linear dependence of $\ln[E_{loc}(T)/kT]$ vs. $\ln T$ gives the value of $-p$. As shown in Fig. 2 (lower panel), the plots of $\ln[E_{loc}(T)/kT]$ vs. $\ln T$ are linear functions within a temperature interval sufficient to determine, above T_{MI}, the values of $p = 0.51 \pm 0.02$ and 0.53 ± 0.02 for the film and the bulk sample,
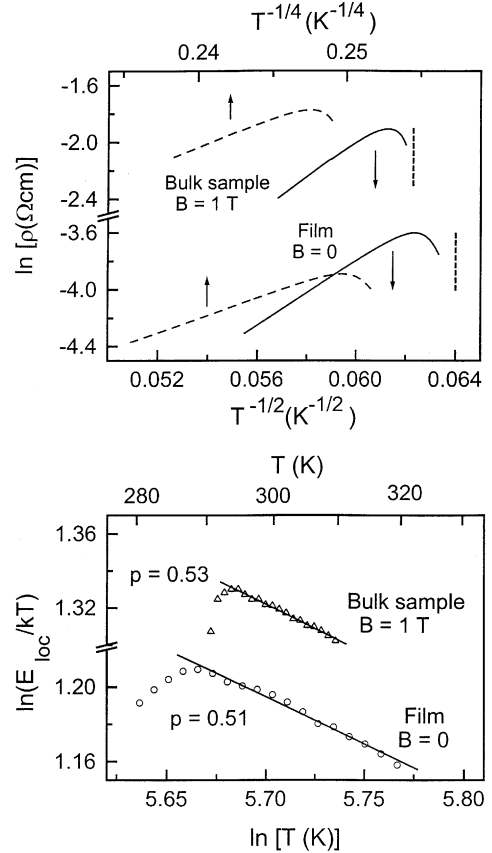

Fig. 2. In the upper panel, the plots of $\ln \rho$ vs. $T^{-1/2}$ (solid lines) and vs. $T^{-1/4}$ (dashed lines) for the thin film at $B = 0$ and the bulk sample at $B = 1$ T are shown. The vertical dotted lines correspond to $T_{MI}^{-1/2}$. In the lower panel, the temperature dependence of the local activation energy, showing the linear fits (solid lines) and the values of p, is given.

respectively, in agreement with the SE–VRH mechanism. In the SE–VRH regime, we can write $\rho_0(T) = \rho_0' T^{1/2}$ [26]. Then, the linear parts of the plots of $\ln[\rho(T)T^{-1/2}]$ vs. $T^{-1/2}$ give $T_0 = 1.74 \times 10^4$ K and $\rho_0' = 5.0 \times 10^{-7}\,\Omega\,cm/K^{1/2}$ for the film at $B = 0$ and $T_0 = 2.15 \times 10^4$ K and $\rho_0' = 1.26 \times 10^{-7}\,\Omega\,cm/K^{1/2}$ for the bulk sample at $B = 1$ T.

At temperatures well below T_{MI}, we fit our resistivity data with the formula for the low-temperature itinerant-carrier resistivity [27]

$$\rho_{lt}(T) = \rho_r + \rho_2 T^2 + \rho_{4.5} T^{4.5}, \tag{3}$$

where ρ_r is the residual temperature-independent resistivity due to scattering by impurities, defects, grain boundaries and domain walls. The second term with the coefficient ρ_2 is ascribed to the electron–electron [17] or single-magnon [28] scattering and the third term with the coefficient $\rho_{4.5}$ to the second-order electron–magnon scattering [29]. As shown in Figs. 3 and 4 (line 2), the resistivity can be fitted below ~ 200 K with Eq. (3) in the film and below ~ 100 K in the bulk sample. The values of the fitting parameters ρ_r, ρ_2 and $\rho_{4.5}$ are given in Tables 1 and 2. In both cases, the dependence of ρ_2 on B is weaker than that of $\rho_{4.5}$. In the film, ρ_r shows no dependence on B, while in the bulk sample, it decreases clearly when B is increased. Similar to the $La_{2/3}Sr_{1/3}MnO_3$ thin film [30], ρ_2 increases and $\rho_{4.5}$ decreases in our film sample when B is increased. In our bulk sample, both ρ_2 and $\rho_{4.5}$ decrease with increasing B as in the $La_{2/3}Sr_{1/3}MnO_3$ thin film [31]. We conclude that $\rho(T)$ can be described in our samples at low temperatures by Eq. (3) using reasonable values and field dependencies of the fitting parameters.

To fit $\rho(T)$ over the temperature interval 10–340 K, we use parallel contributions [10] of $\rho_{ht}(T)$ and $\rho_{lt}(T)$ given by Eqs. (2) and (3),

respectively, as

$$\rho(T) = \{f(T)/\rho_{lt}(T) + [1 - f(T)]/\rho_{ht}(T)\}^{-1}, \quad (4)$$

where $f(T) = \{[\exp(T - T_c^M/\Delta) + 1]^{-1}$ is the fraction of the carriers in the metallic state. Here, the MIT temperature is denoted as T_c^M and Δ is the effective width of the transition interval around T_c^M. In Fig. 3, the contributions from $\rho_{ht}(T)$ (line 1), $\rho_{lt}(T)$ (line 2) and the curve evaluated with Eq. (4) (line 3) for the thin film are shown. The values of ρ_r, ρ_2 and $\rho_{4.5}$ are given in Table 1, and only minor variations of T_0 and ρ_0' (within $\sim 5\%$) with increasing B are required to obtain the best fits with the experimental data. The values of T_c^M and Δ are shown in Table 1, both increasing in an almost linear way with increasing B. As can be seen from Fig. 4, a good fit of $\rho(T)$ can be obtained also for the bulk sample, where the variations of T_0 and ρ_0' with B are negligible. The values of T_c^M and Δ for the bulk sample are shown in Table 2, exhibiting the same behavior as in the film. However, the fits of $\rho(T)$ to the experimental results for the bulk sample require values of ρ_r and ρ_2 (shown in parenthesis in Table 2) differing by 10–40% from those obtained in the low-temperature region, while $\rho_{4.5}$ vanishes for
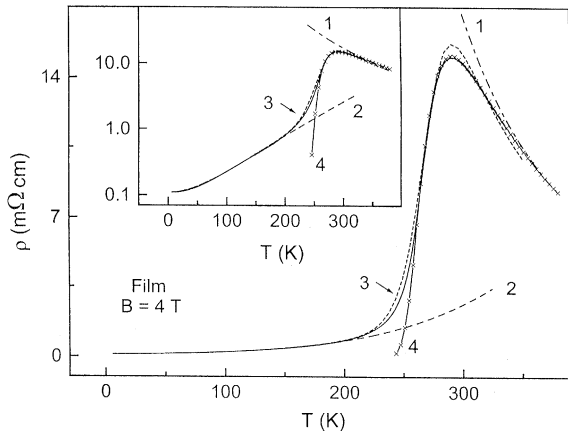

Fig. 3. Experimental dependence of ρ on T in the film at $B = 4$ T (solid line). Line 1 is calculated using Eq. (1) for T_0 independent of T. Line 2 represents the fits of $\rho(T)$ below 200 K with Eq. (3). Line 3 gives the best fit of the whole $\rho(T)$ curve with Eq. (4). Line 4 shows the fit of $\rho(T)$ at $T \geqslant T_{MI}$. The inset shows the same plots in the semi-logarithmic scale.

Fig. 4. Experimental dependence of ρ on T in the bulk sample at $B = 2$ T (solid line). Line 1 is calculated using Eq. (1) for T_0 independent of T. Line 2 represents the fit of $\rho(T)$ below 100 K with Eq. (3). Line 3 gives the best fit of the whole $\rho(T)$ curve with Eq. (4). Line 4 shows the fit of $\rho(T)$ at $T \geqslant T_{MI}$. The inset shows the same plots in the semi-logarithmic scale.
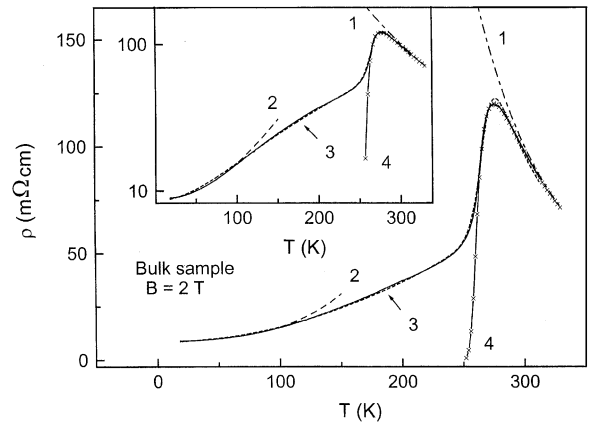
Table 1
The values of the coefficients in Eq. (3), the critical temperature T_C, the width of the transition region Δ in Eq. (4), T'_{MI} and T_{infl}, as determined using Eqs. (1) and (6) and those of T_{MI} and v obtained from the critical behavior of resistivity on the metallic side of MIT in the La$_{0.7}$Ca$_{0.3}$MnO$_3$ thin film

B (T)	ρ_r ($10^{-4}\,\Omega\,cm$)	ρ_2 ($10^{-9}\,\Omega\,cm/K^2$)	$\rho_{4.5}$ ($10^{-14}\,\Omega\,cm/K^{4.5}$)	T_c^M (K)	Δ (K)	T'_{MI} (K)	T_{infl} (K)	T_{MI} (K)	v
0	1.105	9.42	1.69	229	5.52	235	244	241	1.05
1	1.106	9.70	1.60	231	7.53	236	248	251	1.06
2	1.106	10.41	1.29	235	8.97	237	252	253	1.05
4	1.104	10.57	1.10	240	13.2	240	261	261	1.07
8	1.105	10.56	0.85	260	18.4	244	277	281	1.05
10	1.106	10.57	0.84	269	21.5	245	283	287	1.06

Table 2
The values of the coefficients in Eq. (3), the critical temperature T_C, the width of the transition region Δ in Eq. (4), T'_{MI} and T_{infl}, as determined using Eqs. (1) and (6) and those of T_{MI} and v obtained from the critical behavior of resistivity on the metallic side of MIT in the ceramic sample of La$_{0.7}$Ca$_{0.3}$MnO$_3$

B (T)	ρ_r ($10^{-3}\,\Omega\,cm$)	ρ_2 ($10^{-7}\,\Omega\,cm/K^2$)	$\rho_{4.5}$ ($10^{-13}\,\Omega\,cm/K^{4.5}$)	T_c^M (K)	Δ (K)	T'_{MI} (K)	T_{infl} (K)	T_{MI} (K)	v
0	11.16 (12.27)	4.73 (6.64)	2.31 (2.07)	250	2.04	250	250	253	1.06
1	9.31 (8.90)	5.55 (7.68)	1.59 (2.95)	256	3.22	248	255	259	0.99
2	8.72 (8.55)	5.01 (6.97)	1.79 (0)	263	5.28	250	260	264	1.08
4	7.59 (7.90)	4.94 (5.61)	0.95 (0)	277	8.50	249	266	272	1.02
8	6.13 (6.30)	3.86 (4.24)	0.84 (0)	304	10.04	254	281	291	1.03

$B \geqslant 2$ T. As evident from Fig. 4, in the bulk sample, $\rho(T)$ has between $T = 100$ and 200 K, a weak bending up, not present in the film. Eq. (4) constructed from the low- and high-temperature asymptotes given by Eqs. (2) and (3) is insufficient to account for this feature of the bulk sample. Taking into account the purely phenomenological nature of the two-component model expressed by Eq. (4), the agreement with the experimental data of $\rho(T)$ is satisfactory.

2.3. Critical behavior of $\rho(T)$ at MIT

For the next, we analyze the behavior of $\rho(T)$ around T_{MI}, separately for $T \to T_{MI} - 0$ and in the whole interval of the insulating phase above T_{MI}, including $T \to T_{MI} + 0$.

The characteristic VRH temperature can be expressed as $T_0 \sim 1/\xi$, where ξ is the localization radius of the carriers in the insulating phase [25]. The constant slopes of the plots of $\ln \rho(T)$ vs.

$T^{-1/2}$ in Fig. 2 reflect the temperature independence of T_0 and ξ, which is violated as T approaches T_{MI}. This can be attributed to phase segregation due to the charge, orbital or spin ordering. Recent theoretical investigations predict a novel phase separation of the FM state into insulating and metallic FM phases [14,15]. NMR investigations [16] provide experimental evidence for these two phases. The phase-separation phenomena are sensitive to the doping level and to the temperature and the magnetic field [14–16]. We consider a two-phase system formed by the main semiconductor (S) matrix with embedded small metallic (M) particles with radius R. Suppose that the carrier concentrations in the S- and M-phase are n_1 and n_2, respectively, where $n_2 \ll n_1$ above T_{MI}. The localization radius of the carriers in the S-phase, ξ_0, does not depend on T. At $T \gg T_{MI}$, when the M phase represents the assembly of M-particles separated by the S regions, the carriers in the M-phase are localized within a scale $\sim R_0$

corresponding to the high-temperature M-particle size, which should be of the order of the interatomic distance. When the temperature is decreased, R is increased and the separate M-particles join in clusters. Near T_C, the typical cluster size is determined by the cluster correlation length L. As R approaches a percolation threshold R_c, L increases according to $L \sim (R_c - R)^{-v}$, where v is the critical exponent of the correlation length. Instead of R and R_c, it is possible to take any other parameter describing the approach of the system to the percolation threshold with increasing R. Here, we choose T and T_{MI}. Taking into account that at $T \gg T_{MI}$, we have $L = R_0$, we can write $L = R_0(1 - T_{MI}/T)^{-v}$. In the critical regime, at T near T_{MI}, the parameter L plays the role of the localization radius of the carriers of the M-phase. Since, in this regime, the growth of the critical cluster is presumably due to absorption of smaller clusters, the carrier concentrations n_1 and n_2 do not depend on T. Then, we have the total localization volume $V = V_1 + V_2$, with $V_1 \sim n_1 \xi_0^3$ and $V_2 \sim n_2 L^3$. It is convenient to define the mean localization length ξ according to $V \sim n\xi^3$ using

$$\xi = \xi_0(1 + \eta\tau^{-3v})^{1/3}. \qquad (5)$$

Here $\eta = (n_2/n_1)(R_0/\xi_0)^3$ and $\tau = 1 - T_{MI}/T$. Since $\eta \ll 1$, at $T > T_{MI}$, the second term in Eq. (5) is negligible and we get $\xi \approx \xi_0$, independent of T. At $T \to T_{MI} + 0$, ξ becomes temperature dependent due to the unlimited growth of τ^{-v}.

Using Eq. (5), $T_0(T)$ can be written as

$$T_0(T) = T_0^*(1 + \eta\tau^{-3v})^{-1/3}, \qquad (6)$$

where $T_0^* \sim 1/\xi_0$ is equal to the temperature-independent part of T_0 obtained from the linear interval of the plots of $\ln\rho(T)$ vs. $T^{-1/2}$. The curves of $\rho(T)$ calculated using Eqs. (1) and (6) are shown in Fig. 1 (dashed lines) and in Figs. 3 and 4 (lines with crosses). In these calculations, η and the MIT temperature (denoted here as T_{MI}') were regarded as fitting parameters. For $v = 1$, we obtain, in the insulating phase down to T_{MI}, an explicit coincidence with the experimental $\rho(T)$ curves. The values of T_{MI}' are collected in Tables 1 and 2 for the film and the bulk sample, respectively. They depend only weakly on B and are smaller than T_{MI} given by the inflection points of

the experimental curves. On the other hand, the inflection points T_{infl} of the calculated curves (see Tables 1 and 2) are very close to those of the experimental plots of $\rho(T)$ and demonstrate the same dependence on B. Hence, the above description is correct in the whole interval of the insulating phase down to $T = T_{MI}$ and fails only below T_{MI} where Eq. (1) is not applicable. Finally, the zero-field values of $\eta = 5.2 \times 10^{-5}$ and 1.55×10^{-5} for the film and the bulk sample, respectively, are much smaller than unity, as suggested above. However, η in Fig. 5 displays a rapid increase when B is increased, exhibiting a quadratic dependence on B, shown by the straight line in the inset to the figure. This demonstrates an increase of the metallic phase with increasing external magnetic field, a property of the intrinsic phase separation due to the ordering effects in LCMO.

At $T \to T_{MI} - 0$, we can expect the critical behavior of $\rho(T)$ to satisfy the scaling law $\rho^{-1}(T) \sim (1 - T/T_{MI})^v$. As follows from Fig. 6, the plots of $\ln[\rho^{-1}(T) - \rho^{-1}(T_{MI})]$ vs. $\ln(1 - T/T_{MI})$ at $T \to T_{MI} - 0$ are linear both in the film and in the bulk sample with very close slopes in different fields (the term $\rho^{-1}(T_M)$ under the logarithm is introduced to assure a finite value of ρ at T_{MI}). In Tables 1 and 2, the values of T_{MI} and
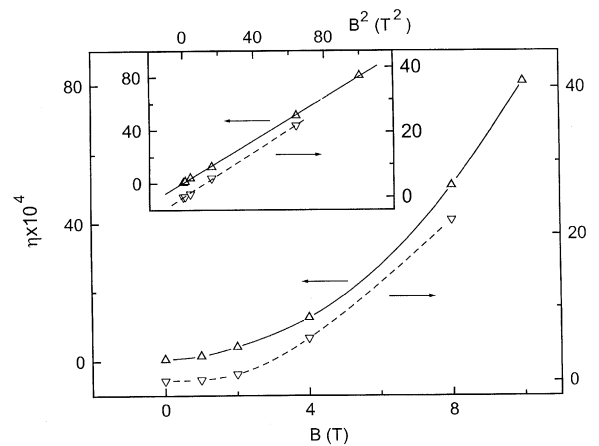

Fig. 5. Dependence of η on B in the thin film ($\triangle$) and in the bulk sample (∇). The solid and the dashed lines are guides to the eye. The inset shows the plots of $\eta(B)/\eta(0)$ vs. B^2, the solid and the dashed lines represent linear fits of the data.
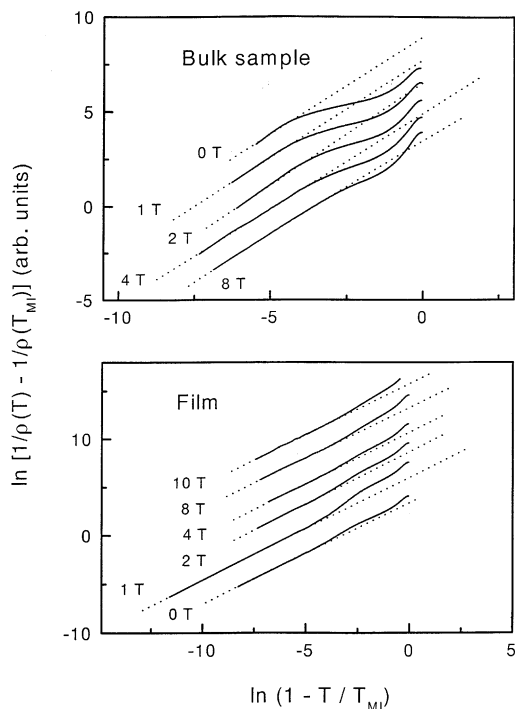
Fig. 6. Plots of $\ln[1/\rho(T) - 1/\rho(T_{MI})]$ vs. $\ln(1 - T/T_{MI})$ for the bulk and the film samples in different magnetic fields. The dotted lines are linear fits of the data calculated using the values of T_{MI} and v given in Tables 1 and 2.

v obtained by fitting the plots in Fig. 6 with linear functions are collected. The values of T_{MI} coincide with those of the inflection points of the experimental $\rho(T)$ curves and v is quite close to unity, in agreement with the value found above T_{MI}. Hence, a consistent description of the critical behavior of $\rho(T)$ is obtained on both sides of MIT.

3. Conclusions

Resistivities of a film and a bulk sample of $La_{0.7}Ca_{0.3}MnO_3$ are investigated between 10 and 340 K in magnetic fields up to 10 T. Well below T_{MI}, the temperature dependence of ρ is determined by two-magnon scattering and electron–electron or single-magnon scattering of itinerant charge carriers. At $T > T_{MI}$, the data of $\rho(T)$ can be explained by the variable-range hopping conductivity and over the whole temperature range of 10–340 K by parallel contributions of localized and itinerant carriers, given by the low- and high-temperature asymptotes of the resistivity. This phenomenological description is accompanied by the analysis of the critical behavior of $\rho(T)$ on both sides of MIT. The critical behavior of the resistivity at $T \to T_{MI} + 0$ is governed by divergence of the carrier localization radius ξ due to the contribution from metallic clusters. The concentration of the metallic phase is increased with increasing magnetic field. On the opposite side of MIT, a scaling behavior of $\rho(T) \sim (T_{MI} - T)^{-v}$ having the same value of the critical exponent $v \approx 1$ as ξ is observed.

References

[1] P. Schiffer, A.P. Ramirez, W. Bao, S.-W. Cheong, Phys. Rev. Lett. 75 (1995) 3336.
[2] A.P. Ramirez, J. Phys.: Condens. Matter 9 (1997) 8171.
[3] C. Meneghini, C. Castellano, A. Kumar, S. Ray, D.D. Sarma, S. Mobilio, Phys. Stat. Sol. B 215 (1999) 647.
[4] M. Hennion, F. Moussa, G. Biotteau, J. Rodriguez-Carvajal, L. Piusard, A. Revcolevschi, Phys. Rev. Lett. 81 (1998) 1957.
[5] A. Mellergård, R.L. McGreevy, S.G. Eriksson, J. Phys.: Condens. Matter 12 (2000) 4975.
[6] M. Jaime, M.B. Salamon, M. Rubinstein, R.E. Treece, J.S. Horwitz, D.B. Chrisei, Phys. Rev. B 54 (1996) 11914.
[7] C.M. Varma, Phys. Rev. B 54 (1996) 7328.
[8] L.-J. Zou, H.Q. Lin, Q.-Q. Zheng, J. Appl. Phys. 83 (1998) 7363.
[9] A.S. Alexandrov, A.M. Bratkovsky, Phys. Rev. Lett. 82 (1999) 141.
[10] M. Rubinstein, J. Appl. Phys. 87 (2000) 5019.
[11] M. Jaime, P. Lin, S.H. Chun, M.B. Salamon, P. Dorsey, M. Rubinstein, Phys. Rev. B 60 (1999) 1028.
[12] J.-M. Liu, Q. Huang, J. Li, C.K. Ong, Z.C. Wu, Z.G. Liu, Y.W. Du, Phys. Rev. B 62 (2000) 8976.
[13] A. de Andres, M. Garcia-Hernandez, J.L. Martinez, Phys. Rev. B 60 (1999) 7328.
[14] S. Yunoki, A. Moreo, E. Dagotto, Phys. Rev. Lett. 81 (1998) 5612.
[15] S. Okamoto, S. Ishihara, S. Makaeva, Phys. Rev. B 61 (2000) 451.
[16] G. Papavassiliou, M. Fardis, M. Belesi, T.G. Maris, G. Kallias, M. Pissas, D. Niarchos, C. Dimitropulos, J. Dolinsek, Phys. Rev. Lett. 84 (2000) 761.
[17] M. Ziese, Phys. Rev. B 62 (2000) 1044.
[18] X.W. Cao, J. Fang, Z.H. Wang, K.B. Li, Appl. Phys. Lett. 75 (1999) 3372.
[19] M. Jaime, M.B. Salamon, M. Rubinstein, R.E. Treece, J.S. Horwitz, D.B. Chrisei, Phys. Rev. B 54 (1996) 11914.

[20] T.T. Palstra, A.P. Ramirez, S.-W. Cheong, B.R. Zegarski, P. Schiffer, J. Zaanen, Phys. Rev. B 56 (1997) 5104.

[21] M. Jaime, H.T. Hardner, M.B. Salamon, M. Rubinstein, P. Dorsey, D. Emin, Phys. Rev. Lett. 78 (1997) 951.

[22] R.M. Thomas, L. Ranno, J.M.D. Coey, J. Appl. Phys. 81 (1997) 5763.

[23] A.I. Coldea, I.M. Marshall, S.J. Blundell, J. Singleton, L.D. Noailles, P.D. Battle, J. Rosseinsky, Phys. Rev. B 62 (2000) R6077.

[24] N.F. Mott, E.A. Davies, Electron Processes in Non-Crystalline Materials, Clarendon, Oxford, 1979.N.F. Mott, Metal–Insulator Transitions, Taylor & Francis, London, 1990.

[25] B.I. Shklovskii, A.L. Efros, Electronic Properties of Doped Semiconductors, Springer, Berlin, 1984.

[26] T.G. Castner, in: M. Pollak, B. Shklovskii (Eds.), Hopping Transport in Solids, Elsevier, Amsterdam, 1991.

[27] G.J. Snyder, R. Hiskes, S. DiCarolis, M.R. Beasley, T.H. Geballe, Phys. Rev. B 53 (14) (1996) 434.

[28] M. Jaime, P. Lin, M.B. Salamon, P.D. Han, Phys. Rev. B 58 (1998) R5901.

[29] K. Kubo, N. Ohata, J. Phys. Soc. Japan 33 (1972) 21.

[30] J.C. Chen, S.C. Law, L.C. Tung, C.C. Chi, W. Guan, Phys. Rev. B 60 (12) (1999) 143.

[31] P. Mandal, K. Barner, L. Haupt, A. Poddar, R. von Helmolt, A.G.M. Jansen, P. Wyder, Phys. Rev. B 57 (10) (1998) 256.